Improving Current Distribution Model for EBWCD using Flux Loops in QUEST

Junyao, Zhou
Interdisciplinary Graduate School of Engineering Sciences, Kyushu University

Hanada, Kazuaki
Research Institute for Applied Mechanics, Kyushu University

Kuroda, Kengoh
Center for Maritime Safety and Security Studies, Japan Coast Guard Academy

Onchi, Takumi
Research Institute for Applied Mechanics, Kyushu University

他

出版情報：Evergreen. 11 (2), pp.555-562, 2024-06. 九州大学グリーンテクノロジー研究教育センター
バージョン：

Improving Current Distribution Model for EBWCD using Flux Loops in QUEST

Zhou Junyao[1*], Hanada Kazuaki[2], Kuroda Kengoh[3], Onchi Takumi[2], Idei Hiroshi[2], Ikezoe Ryuya[2], Hasegawa Makoto[2], Nagashima Yoshihiko[2], Ido Takeshi[2], Kinoshita Toshiki[2]

[1]Interdisciplinary Graduate School of Engineering Sciences, Kyushu University, Fukuoka, Japan

[2]Research Institute for Applied Mechanics, Kyushu University, Fukuoka, Japan

[3]Center for Maritime Safety and Security Studies, Japan Coast Guard Academy, Hiroshima, Japan

E-mail: j.zhou@triam.kyushu-u.ac.jp

(Received March 6, 2024; Revised May 6, 2024; Accepted May 31, 2024).

Abstract: During the early phase of tokamak plasma start-up prior to the formation of a closed magnetic surface, various plasma current profiles are expected to be observed. Especially, the non-inductive current drive (CD) by the electron Bernstein wave (EBW) is likely to be the most dominant, and the current profile is expected to focus on a local area predicted by the theoretical model. In addition, the EBWCD direction could be affected by a horizontal magnetic field induced by a toroidal magnetic field coil and feed-through. The magnetic flux data cannot be fitted by using a previous model described by Yoshinaga[23], and hence, this model needs improvement. Consequently, an improved model is introduced in this paper based on the theoretical prediction of EBWCD. This model can be applied to reproduce the complex plasma current profile accurately during the early phase of the tokamak plasma start-up.

Keywords: Electron Bernstein Wave; HFS injection; current drive; early phase of tokamak plasma start-up model of current profile

1. Introduction

Nuclear fusion power has been considered as an ultimate solution for energy crisis[1)2)3)], in which spherical tokamak (ST) has higher economic benefits than traditional tokamak device. For fusion reactors in low aspect ratio devices such as ST, a non-inductive method for plasma start-up is required due to the limited space for the center solenoid coils in the central part of the torus. In this regard, RF injection is considered as a promising method. Due to the higher dielectric constant in present STs as compared to those in conventional tokamaks, the electron cyclotron wave (ECW), which has been used to be applied to tokamak plasma start-ups[4)5)], is less effective in STs. On the other hand, the electron Bernstein wave (EBW) is more appropriate than ECW for the plasma start-up in STs because EBW can propagate in high-density plasma as an electrostatic wave and can be effectively absorbed even in low-temperature plasma[6)7)8)9)].

EBW-assisted plasma current start-up has been used in several devices. Electron Bernstein heating (EBH) experiments in the COMPASS-D device have proved that the heating efficiency reaches the maximum at vertical injection[10)11)12)]. EBW-assisted plasma start-up by HFS injection has been successfully achieved in QUEST device[13)14)15)16)]. The existence of EBWCD was proved based on the anti-phase response of the plasma current, I_p, to the vertical modulation of the plasma mid-plane by changing the PF coil current during (radio frequency) RF injection in the MAST device[17)18)19)]. EBWCD will be generated in opposite directions due to the opposite radial magnetic field, B_R, on the two sides of the plasma mid-plane when the EBW is injected vertically based on the calculation by Maekawa et al.[20)]. In this case, if the EBWCD is in the same direction as that of the pressure-driven current, the formation of a closed flux surface (CFS) may be favored. If the EBWCD is in the opposite direction to that of the current, it may cause a hindrance to the formation of a CFS. Therefore, determining the optimal magnetic field configuration may improve the efficiency of the EBWCD. However, prior to that, an appropriate current profile model needs to be developed to determine the amount of current that flows in the same direction as that of the pressure-driven current or the opposite direction to that of the current. D.W. Swain et al.[21)] and G.L. Jackson et al.[22)] used several filaments models to fit the current profile in the CFS phase in ECCD experiments. Yoshinaga et al.[23)] and Kuroda et al.[24)] used the elliptical distribution model and D-shaped distribution

model to effectively fit the pressure-driven current profile in both the open flux surface (OFS) and CFS phases in ECCD experiments. However, the measured plasma current is a mixture of EBWCD and pressure-driven current, and so far, no model exists that can describe EBWCD effectively, especially in the OFS phase.

Therefore, this study attempted to improve the Yoshinaga model to better fit the current distribution predicted by the theoretical model for EBWCD in the configuration of QUEST. The magnetic diagnostics equipped in QUEST are used in the calculation, and the expected observations are introduced.

2. Experimental and measure apparatus

The QUEST is a spherical tokamak with $R_0 = 0.64$m and $a = 0.36$ m, as shown in Fig.1. Eight 2-turn TF coils are installed outside the vacuum vessel. When a current of 50 kA flows through the coil, a toroidal magnetic field of 0.25 T is formed at $R = 0.64$ m. Five pairs of PF coils (10 in total) are arranged symmetrically in the upward and downward directions with the equatorial plane of the vacuum vessel. A pair coil, referred to as HCUL coils, with currents of the same magnitude and opposite directions is used to generate a horizontal magnetic field for adjusting the vertical position of the plasma.

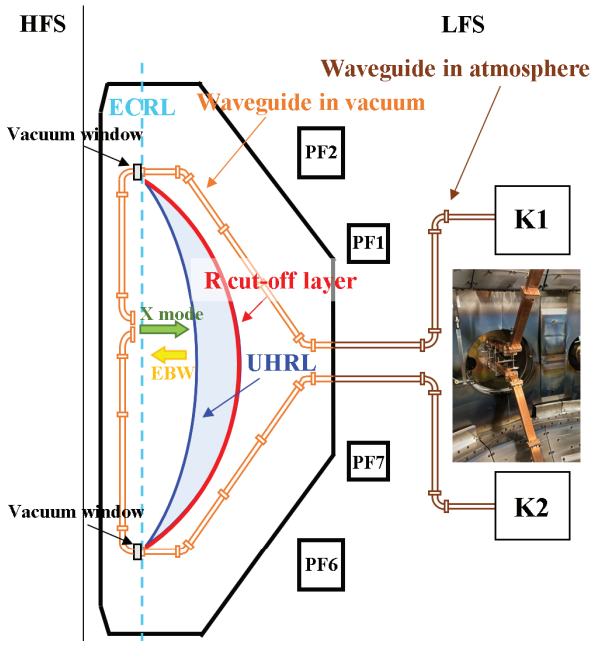

Fig. 1: Right cross-sectional view of QUEST to explain the position of poloidal field coils and the process of the X-B mode conversion. . The vacuum vessel was carefully evacuated with several pumps to make plasmas. In the experiments, only symmetrically located coils that PF1 &PF7, PF2 & PF6 were employed. The additional waveguides were inserted through a horizontal port and its vacuum side is connected to an antenna and the other side is connected with a CW klystron of 8.2 GHz and 25 kW. The ECW launched from HFS is converted into EBW when reached at the vicinity of UHR layer and the EBW is propagating toward HFS.

In a typical configuration of the tokamak plasma start-up, no plasma is located inside the vacuum vessel initially, and an RF wave is injected to form a plasma. The RF wave can propagate as an electro-magnetic wave and meets the electron cyclotron resonance (ECR) layer, where the RF frequency matches the electron gyro-frequency and can accelerate electrons. The accelerated electrons collide with neutral particles, and the ionization of the neutral particles actively occurs at the ECR layer. Finally, an avalanche of ionization takes place, and plasma break-down occurs. After the plasma break-down, the presence of plasma modifies the wave-particle interaction. The injected RF that propagates as the X-mode cannot reach the ECR layer from the low-field side due to cut-off property. However, the RF wave from the high-field side can pass through the ECR layer and reach upper hybrid resonance (UHR) layer. The RF wave is converted into an electrostatic wave called EBW. The EBW exhibits a good capability to heat low-temperature plasma efficiently and drive plasma current that is important to make a CFS.

In the experiment, PF coils 1-7 (-29.9 A×12 turns) and 2-6 (166.7 A×36 turns) are used to create a vertical magnetic field of $B_v = 2$ mTand $n - index = 0.35$ at $R = 0.6$ m on the equatorial plane[25]. Two klystrons with 20kW/8.2GHz power output each are employed to inject eXtra-ordinary (X-) mode ECW perpendicularly to the magnetic field from the antennas located 0.17m above equatorial plane. The ECW is converted into EBW when reached at the vicinity of UHR layer and the EBW is propagating toward HFS. The EBW is expected to be absorbed near the ECR layer. RF is launched from 0 to 0.22s and amplitude modulation is conducted from 0.1s to investigate the influence of EBW on plasma current.

MI cables are used for magnetic diagnostics. The MI cables with excellent heat and vacuum resistance are used as conductor wires, which are wound into loops on the vacuum vessel wall and in the center stack to make flux loop coils. The vertical magnetic flux generated by the plasma current and PF coils current during RF injection is measured by flux loop coils as shown in Fig.2.

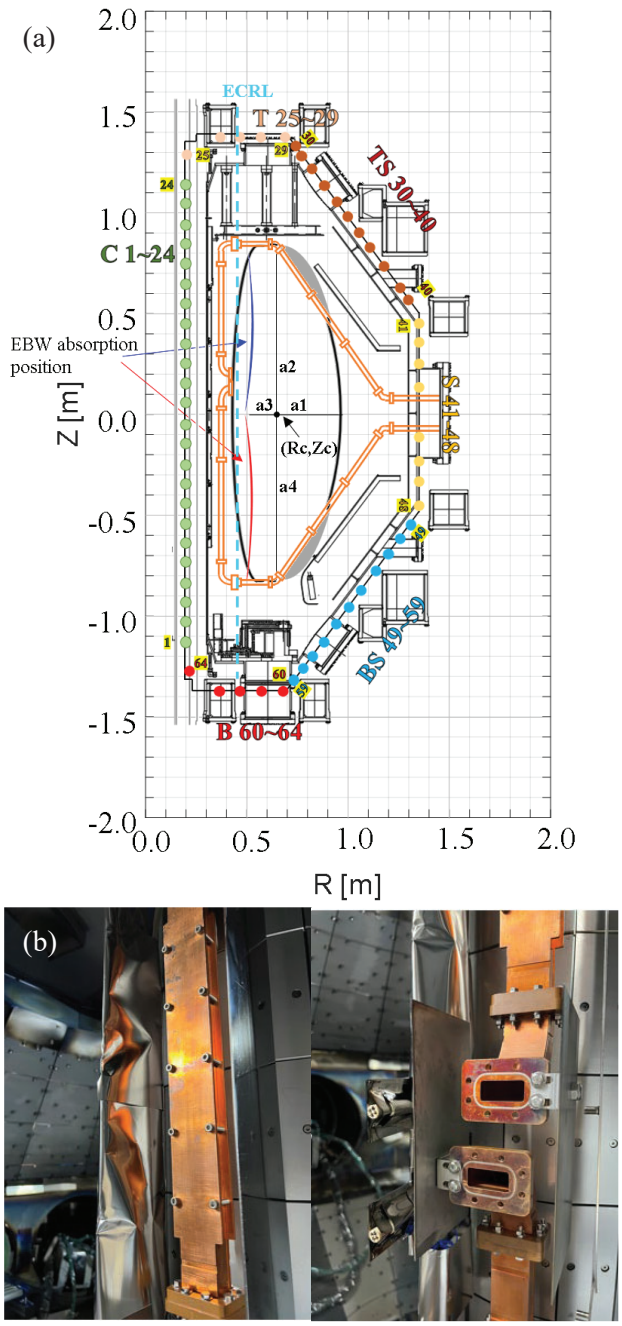

Fig. 2: (a) Magnetic flux loops distributed in vacuum vessel wall and the location of predicted EBW absorption position, in which the blue part represents where the EBWCD generated in CW and the red part represents where the EBWCD generated in CCW. The elliptical outline represents the current profile of Yoshinaga model[23]. The area in gray denotes that current density is set as zero due to the limitation effect of waveguides. (b) The photos of the covers of waveguides on the center stuck side. The width of covers is 0.1 m. The presence of the cover has been considered in the models as the plasma current edge, where the current density is possible to be 0.

Based on Faraday's law of electromagnetic induction,

$$E_{FL} = -\frac{d\Psi}{dt},$$

where E_{FL}[V] denotes the output voltage of the flux loop coil, and ψ[Wb] denotes the vertical magnetic flux passing through the flux loop coils. When the plasma current or PF coil current changes, the vertical magnetic flux passing through the flux coil will change, causing a voltage signal to be generated on the coil. By integrating the voltage signal collected by the oscilloscope over time, the vertical magnetic flux at the magnetic flux coil at any time can be obtained. On the center stack, there are flux loop coils located every 0.1 m from $Z = 1.15$ m to -1.15 m, 24 in total. Since these 24 coils are much closer to the predicted ECRL ($R = 0.45$ m) and EBW absorption positions than the other flux loop coils, they are connected to an oscilloscope (DL850 type Yokogawa Electric Corp.) with a higher sampling frequency of 100 KS/S. However, when the current contains high-frequency noise with a frequency that is higher than the sampling frequency, a measurement error called drift occurs. To obtain the plasma-induced magnetic signal caused by the plasma current, off-shots, which have the same magnetic configuration without RF injection, are conducted to measure the background of the magnetic flux generated by the PF coils current, subtract the magnetic component caused by the PF coils from the integrated magnetic flux curve, and subsequently, use a linear function that subtracts the drift component due to the plasma current from the curve.

The magnetic flux was measured during the shots with and without RF injection under the same magnetic configuration, then the data of the shot with RF injection was reduced by the data of the shot without RF injection to obtain the pure magnetic flux generated by plasma current. Figure 3 shows the measured plasma current and pure magnetic flux distribution from Ch.1 to Ch.24 denoted in Fig. 2 under the magnetic configuration at B_T of 0.22 T, CCW direction from the top view and at B_v of 0.002 T, upward. It should be moted that these magnetic fields kept constant during the discharge. The direction of plasma current identifies the positive values are CCW and the negative ones are CW from the top view. The RF power of 50 kW was injected at the time of 0 sec and the plasma current came up just after the RF injection. Subsequently, the plasma current kept constant for more than 40 ms, which is considered as an OFS phase. Then plasma current jumped suddenly to four times larger. This phenomena has been recognized as current jump to form a CFS[26)27)]. The proposed current distribution models is developed to apply to the data around 0.02s to avoid the influence of eddy current on the vacuum vessel caused by quick RF start-up, because there is no current distribution model for EBWCD in OFS at the plasma start-up phase.

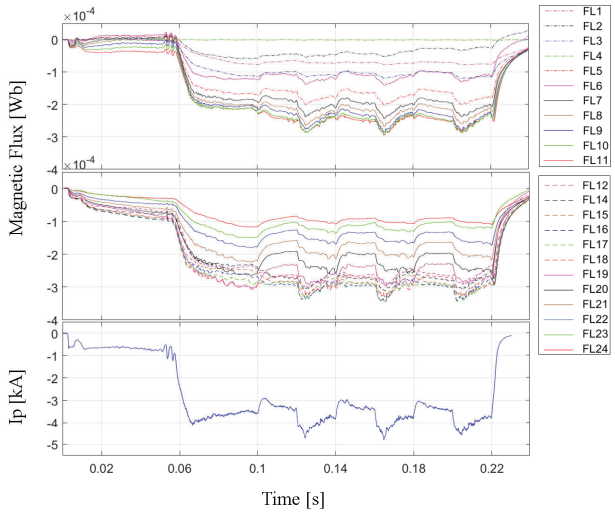

Fig. 3: Measured plasma current and magnetic flux distribution from Ch.1 to Ch.24 under the magnetic configuration at B_T of 0.22 T, CCW direction from the top view and at B_v of 0.002 T, upward. There was no signal in FL4 and FL13.

3. Estimation model

The model used in this study has been described in a previous paper[23]. As shown in Fig. 2, the model assumes a power law parabolic profile. In the upper right-hand side portion from the center of the ellipse, the current density (j) is given as,

$$j = j_0 \cdot [1 - \frac{(R - R_c)^2}{{a_1}^2} - \frac{(Z - Z_c)^2}{{a_2}^2}]^{\alpha}$$

And the current density (j) in the lower left-hand side portion is given as,

$$j = j_0 \cdot [1 - \frac{(R - R_c)^2}{{a_3}^2} - \frac{(Z - Z_c)^2}{{a_4}^2}]^{\alpha}$$

A total of 7 parameters are used to fit the measurement data of 64 flux loop coils, and the optimal parameter values are estimated. For these seven parameters, (R_c, Z_c) is the center coordinate of the elliptical current profile and is also the position of the current density peak. j_0 represents the current density peak, (a_1, a_2, a_3, a_4) are the four radii of the elliptical profile, and α represents the decay coefficient of the current density toward the boundary. The currents are expected to flow in the same direction within the elliptical region and exhibit a smooth decay toward the region boundaries. At the same time, since the waveguides inside the vacuum vessel in this experiment played the same role as that of the limiters, the electrons impacted on the waveguide, and the current could not be formed. Therefore, within the scope of the vessel, the current density profile is cut off at the waveguide. The current density outside the waveguides is assumed to be zero as shown in Fig.2 (a). The covers of the waveguides on the center stuck with the width of 0.1 m have also been considered in the models as the plasma current edge, where the current density is possible to be 0.

In this way, the vertical magnetic flux passing through the coil at any position can be calculated for any parameter set. For instance, the magnetic flux passing through the k_{th} coil is given as

$$\psi_k = M_k(R_c, Z_c, a_1, a_2, a_3, a_4, \alpha) \cdot \int j \, \mathrm{d}R \, \mathrm{d}Z$$

Here, the M_k represents the mutual inductance between the k_{th} coil and plasma current. The square root error ϵ between the measured magnetic flux ${\psi_k}^P$ and the calculated magnetic flux ψ_k is defined as

$$\epsilon = (\frac{\sum_k [\sigma_k(\psi_k - {\psi_k}^P)]^2}{\sum_k (\sigma_k {\psi_k}^P)^2})^{1/2}$$

Here, σ_k is the weight coefficient of each flux loop coil. In this study, the weight coefficient of all the coils is set as the same. If a set of parameters $(R_c, Z_c, a_1, a_2, a_3, a_4, \alpha)$ can be found that best matches the measured value of the magnetic flux with the calculated value and has the smallest error, it implies that the current density profile corresponding to this parameter set best matches the experimental measurement and is closest to the actual current profile. For this purpose, 7 parameters are scanned within a certain range, where the range of (R_c, Z_c) is limited to the waveguide, the resolution is 10 cm, the value of α ranges from 1 to 2, and the resolution is 0.05.

However, based on the magnetic field configuration in experiments, an EBW current always exists in a direction that is opposite to that of the pressure-driven current on the upper or lower side of the midplane due to the opposite B_R generated by the pairs of PF coils. However, the Yoshinaga current profile model involves only one direction; therefore, the improvement of the model is necessary for the simulation and reappearance of the EBWCD in the opposite direction.

According to the predicted EBW absorption position, filaments can be added to represent the EBW current in a concentrated manner, or a strip-shaped approximate distribution of current can be added to represent the EBW current that is continuously generated due to the absorption of EBW in that region. The illustrations of two models are shown in Fig. 4

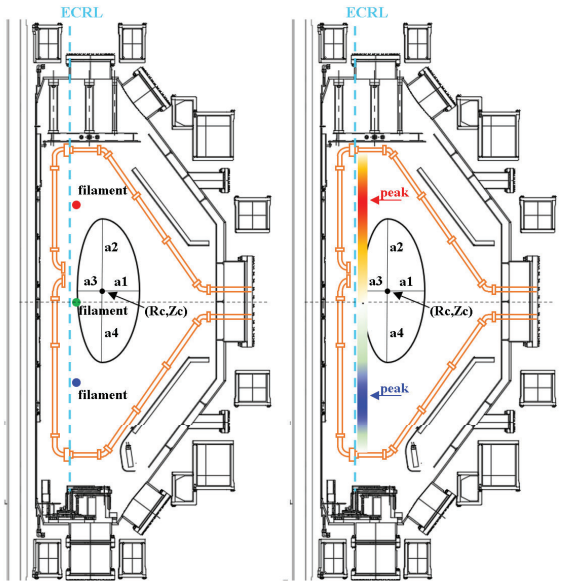

Fig. 4: Illustrations of two kinds of models. Left: filament model. Three filaments will be set at the EBW absorption position and mid-plane. Right: strip model. The parts above and below the equatorial plane represent the current in opposite directions. Peaks in both parts represent the maximum of EBW current density and current density decays toward upper and lower sides if the decay coefficient is applied.

In the filaments current model, three filaments will be set at the EBW absorption position and mid-plane. Due to the narrow size of the EBW absorption position from R=0.46 m to 0.48 m, the position of R has a neglectable influence as compared to the Z position and magnitude of the filaments. The number of filaments will be adjusted according to the fitting results.

However, the current in the filaments will result in undesirable bending on the magnetic surface due to the over-concentration if the magnitude is large with respect to the pressure-driven current. In this situation, a strip current model will be a better option. In the strip current model, the EBW current is distributed from R=0.46 m to 0.48 m and Z=0.75 m to -0.75 m (limitation of waveguides). The current above or below the mid-plane is in an opposite direction and has different parameters such as the Z location of the peak position and decay coefficient. The EBW current in this model will not decay on the R axis due to the narrow size. However, on the Z axis, fitting will be conducted with and without the decay coefficient because the real absorption location and diffusion behavior of EBW in the experiments is unknown. Limited by the accuracy of measurements and estimation model, the decay of the current density profile of EBW cannot be determined if the calculation fits the measurement data effectively without a decay coefficient.

The magnetic flux of the k_{th} coil should be

$$\psi_k = M_k \cdot \int j \, dR \, dZ + M_k^E \cdot I_{\mathrm{EBW}}$$

Here, I_{EBW} represents the EBWCD in the filaments or the strip-shaped profile, and M_k^E represents the mutual inductance between the k_{th} coil and the EBW current.

Figure 5 shows the influence of different models with the same magnitude of EBW current on magnetic flux distribution, in which the pressure-driven current was set as -650 A. The calculation result obtained by using only the Yoshinaga model is represented by black spots. Then EBW current with different models was applied in the basis of black spots.

In order to compare the effect of different models without affecting the total current, the EBW current represented by the filaments or the strips was set symmetrically above and below the mid-plane with the amount of ±70 A (blue symbols), ±140 A (orange symbols), and ±210 A (red symbols), respectively. The negative and positive current were in the CCW and CW direction, and generated magnetic flux in negative and positive values. The positive current was set above the mid-plane, and the negative one was set below it. The circle symbols and triangle symbols denote the calculation results obtained by adding the EBW current in the filaments or the strips on the basis of the Yoshinaga model. In this calculation, the EBW current density in the strips decayed from the peak position until attaining the value of 0 A at the mid-plane. The calculation revealed that the effect of EBWCD could be detected by measuring the magnetic flux only when the EBW current was large enough (near 70 A or much larger).

The magnetic flux of the EBW current in the strip-model exhibited more difference when the direction of the current was the same as that of the pressure-driven current (around Ch.15and Ch.42). However, the EBW current in the direction opposite to that of the pressure-driven current could be observed more easily using the filament-model (around Ch.6).

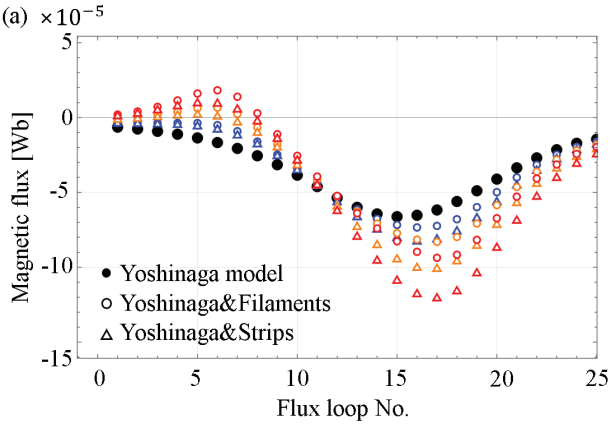

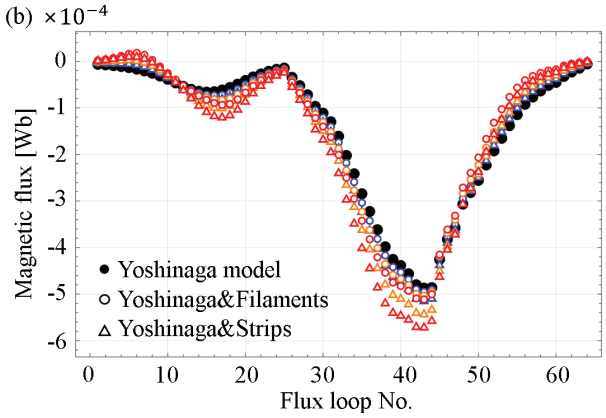

Fig.5: Magnetic flux calculated by different models, in which the pressure-driven current is set as -650 A. The EBW current is ±70 A in blue symbols, ±140 A in orange symbols, and ±210 A in red symbols. The black spots denote that only the Yoshinaga model is used. The circle and triangle symbols denote that the EBW current is in the filament-model or strip-model. Figure (a) shows the partial enlargement of Fig. (b) from Ch.1 to Ch.24.

The examples of estimated current profile by each model is shown in Fig. 6. The left figure shows the profile with strip model, the right figure shows the one with filament model. The magnitude of current density in these profiles has taken the logarithm to avoid the huge difference between current density of filament or strip model and Yoshinaga model. The total current of EBW current in filament and strip model has been noted. And the corresponding magnetic flux distribution nearby the Center stuck is shown in Fig. 6.

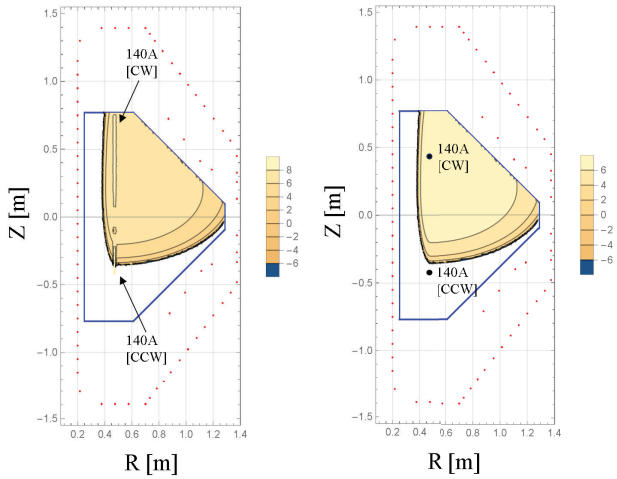

Fig. 6: Estimated current profile using the magnetic flux data in Fig. 3 by each model. The left figure shows the strip model, the right figure shows the filament model.

The magnetic flux distribution of results in Fig. 6 by the filament model and the strip model are shown in Fig. 7.

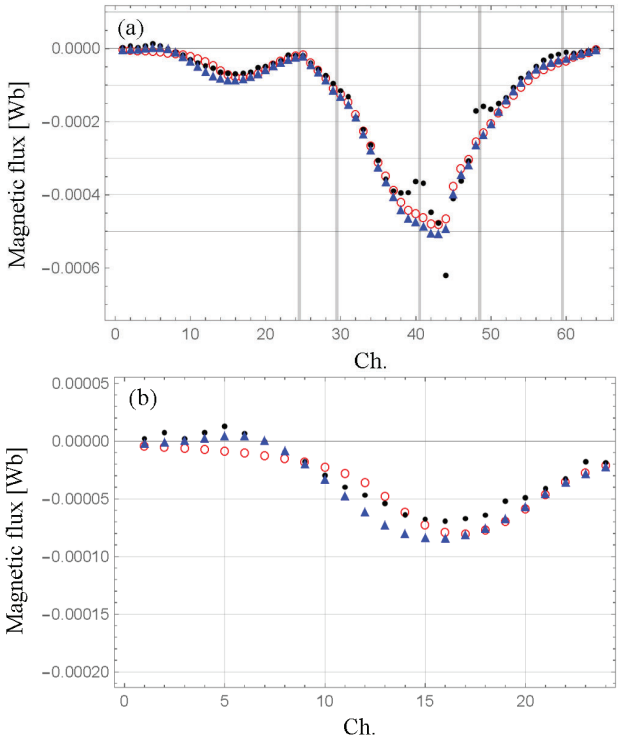

Fig. 7: Fitting results based on the data in Fig. 2 by the filament model and the strip model. The black spots represent the measured magnetic flux, the blue symbols represent the fitting result by the filament model and the red ones by the strip model. (a) shows the results of 64 channels and (b) shows the partial enlargement from Ch.1 to Ch.24. It should be noted that the data in the range of ch39-41 and ch49-51 were not used for the fitting due to the large deviation from the calculated results, although the reason is unclear.

The black spots represent the measured magnetic flux, the blue symbols represent the fitting result by filament model and the red ones by the strip model. It can be noticed that filament model matched measurement data better in the lower half of vacuum vessel (before Ch.12), where the EBW current is opposite to the pressure driven current. Therefore, EBW current might be concentrated in that region.

This result indicates that the magnetic flux loops equipped on QUEST can be detected by the presence of the plasma current driven by the EBW. Especially, the magnetic flux loops located on the center stuck are important for noting the difference because EBW is expected to be absorbed nearby the ECR layer which is closed to the center stuck. The calculation is helpful for the preparation of the measurement prior to the experiment.

3. Summary

In the case of EBW-assisted plasma current start-up, the total plasma current is composed of pressure-driven current and EBWCD. If the EBWCD is in the same direction as that of the pressure-driven current, the formation of CFS is promoted, while the opposite case

may disrupt this process. In order to determine the distribution and magnitude of EBWCD in each direction, this study adds the EBW current models according to the predicted EBW absorption position on the basis of the pressure-driven current profile model. Two kinds of EBW current model are proposed: one is filament, and the other one is the strip-shade model with much larger calculations. The filament model can simply represent the magnitude and center position of the EBW current generated in the upper and lower half of vacuum vessel. If EBW current is concentrated, it is better to use the filament model because the required calculation is much smaller compared to strip mode since there are fewer parameters to be fitted. However, the filament model is not suitable when EBW current is respectively dispersed or becomes large because the concentration current in filament will result in a small CFS around filament and the strange bending of magnetic surface. The strip model is better in this situation though it needs larger calculation due to more fitting parameters. These two models show an obvious difference in the results obtained for the cases where the currents were in the same or opposite direction to that of the pressure-driven current. Therefore, both have the flexibility of application for fitting the measured magnetic flux data by flux loop coils set in QUEST.

Acknowledgements

This work was part-funded by the JST SPRING (Grant No.JPMJSP2136).

References

1) Yoneda, Ryota. "Research and technical trend in nuclear fusion in japan." EVERGREEN, 4 (4) 16-23 (2017). doi.org/10.5109/1929677
2) Barai, M. K., & Saha, B. B. "Energy security and sustainability in japan." EVERGREEN, 2(1): 49-56 (2015). doi.org/10.5109/1500427
3) Fujisaki, T. "Evaluation of green paradox: case study of japan." (2018): 26-31.
4) Y. Takase, A. Ejiri1, H. Kakuda, Y. Nagashima, T. Wakatsuki, O. Watanabe1, P. Bonoli, O. Meneghini, S. Shiraiwa, J. Wright, C. Moeller, H. Kasahara, R. Kumazawa, T. Mutoh, K. Saito and TST-2 Group, "Development of a plasma current ramp-up technique for spherical tokamaks by the lower hybrid wave." Nuclear Fusion 51.6 (2011): 063017.
5) Luce, T. C., et al. "Generation of localized noninductive current by electron cyclotron waves on the DIII-D tokamak." Physical review letters 83.22 (1999): 4550.
6) Bernstein, Ira B. "Waves in a plasma in a magnetic field." Physical Review 109.1 (1958): 10.
7) Ram, A. K., and Steven Donald Schultz. "Excitation, propagation, and damping of electron Bernstein waves in tokamaks." Physics of Plasmas 7.10 (2000): 4084-4094.
8) Taylor, G., et al. "Efficient generation of noninductive, off-axis, Ohkawa current, driven by electron Bernstein waves in high β, spherical torus plasmas." Physics of plasmas 11.10 (2004): 4733-4739.
9) Urban, Jakub, et al. "A survey of electron Bernstein wave heating and current drive potential for spherical tokamaks." Nuclear Fusion 51.8 (2011): 083050.
10) Shevchenko, V., Baranov, Y., O'brien, M. and Saveliev, A. "Generation of noninductive current by electron-Bernstein waves on the COMPASS-D tokamak." Physical review letters 89.26 (2002): 265005.
11) Shevchenko, V., G. Cunningham, and A. Field. "EBW emission observations on COMPASS-D and MAST." Proc. 28th EPS Conf. Controlled Fusion and Plasma Physics. (2001): 1285-2001.
12) Shevchenko, V., et al. "Electron Bernstein Wave Studies on COMPASS - D and MAST." AIP Conference Proceedings. American Institute of Physics. (2003), 694(1): 359-366.
13) Idei, Hiroshi, et al. "ECW/EBW heating and current drive experiment results and prospects for CW operation in QUEST." Plasma and Fusion Research 7 (2012): 2402112-2402112.
14) Yoneda, Ryota, et al. "High-field-side RF injection for excitation of electron Bernstein waves." Plasma and Fusion Research 13 (2018): 3402115-3402115.
15) Hatem Elserafy, Kazuaki Hanada, Shinichiro Kojima, Takumi Onchi, Ryuya Ikezoe , Kengoh Kuroda, Hiroshi Idei, Makoto Hasegawa, Ryota Yoneda, Masaharu Fukuyama, Arseniy Kuzmin, Aki Higashijima, Takahiro Nagata, Shoji Kawasaki, Shun Shimabukuro, Nicola Bertelli and Masayuki Ono, "Electron Bernstein wave conversion of high-field side injected X-modes in QUEST." Plasma Physics and Controlled Fusion 62.3 (2020): 035018.
16) Hatem ELSERAFY, Kazuaki HANADA, Kengoh KURODA, Hiroshi IDEI, Ryota YONEDA, Canbin HUANG, Shinichiro KOJIMA, Makoto HASEGAWA, Yoshihiko NAGASHIMA, Takumi ONCHI, Ryuya IKEZOE, Aki HIGASHIJIMA, Takahiro NAGATA, Shoji KAWASAKI, Shun SHIMABUKURO, Nicola BERTELLI and Masayuki ONO, "HFS injection of X-mode for EBW conversion in QUEST." Plasma and Fusion Research 14 (2019): 1205038-1205038.
17) Shevchenko, V., et al. "Development of electron Bernstein wave research in MAST." Fusion science and technology 2007, 52(2): 202-215.
18) Shevchenko, V. F., Baranov, Y. F., Bigelow, T., Caughman, J. B., Diem, S., Dukes, C., Finburg, P., Hawes, J., Gurl, C., Griffiths, J., Mailloux, J., Peng, M., Saveliev, A. N., Takase, Y., Tanaka, H. and Taylor, G. "Long pulse EBW start-up experiments in MAST." EPJ Web of Conferences. EDP Sciences, (2015), 87: 02007.

19) Shevchenko, V. F., et al. "Electron Bernstein wave assisted plasma current start-up in MAST." Nuclear Fusion 2010, 50(2): 022004.
20) Maekawa, T., H. Tanaka, and M. Uchida. "Mapping of power deposition zone of electron Bernstein waves externally excited in tokamak plasmas." Plasma Physics and Controlled Fusion 61.10 (2019): 105017.
21) Swain, D. W., and G. H. Neilson. "An efficient technique for magnetic analysis of non-circular, high-beta tokamak equilibria." Nuclear Fusion 22.8 (1982): 1015.
22) Jackson, G. L., Humphreys, D. A., Hyatt, A. W., Lohr, J. M., Luce, T. C., & Yu, J. H. "Noninductive plasma initiation and startup in the DIII-D tokamak." Nuclear Fusion 51.8 (2011): 083015.
23) Yoshinaga, T., Uchida, M., Tanaka, H., & Maekawa, T. "A current profile model for magnetic analysis of the start-up phase of toroidal plasmas driven by electron cyclotron heating and current drive." Nuclear fusion 47.3 (2007): 210.
24) Kuroda, K., Wada, M., Uchida, M., Tanaka, H., & Maekawa, T. "Shift in principal equilibrium current from a vertical to a toroidal one towards the initiation of a closed flux surface in ECR plasmas in the LATE device." Plasma Physics and Controlled Fusion 58.2 (2016): 025013.
25) R. Yoneda, K. Hanada, K. Nakamura, H. Idei, N. Yoshida, M. Hasegawa, T. Onchi, K. Kuroda, S. Kawasaki, A. Higashijima, T. Nagata, A. Isayama, O. Mitarai, A. Fukuyama, and Y. Takase, "Effect of magnetic structure on RF-induced breakdown in QUEST." Physics of Plasmas 24.6 (2017).
26) Yoshinaga, T., Uchida, M., Tanaka, H., & Maekawa, T. "Spontaneous formation of closed-field torus equilibrium via current jump observed in an electron-cyclotron-heated plasma." Physical review letters 96.12 (2006): 125005.
27) Uchida, M., Maekawa, T., Tanaka, H., Ide, S., Takase, Y., Watanabe, F., & Nishi, S. "Generation of initial closed flux surfaces by ECH at a conventional aspect ratio of R/a~ 3: experiments on the LATE device and JT-60U tokamak." Nuclear Fusion 51.6 (2011): 063031.